Nanoscale Research Letters
a SpringerOpen Journal

NANO EXPRESS

Open Access

CrossMark

Dilute Magnetic Semiconductor and Half-Metal Behaviors in 3*d* Transition-Metal Doped Black and Blue Phosphorenes: A First-Principles Study

Weiyang Yu[1,2], Zhili Zhu[1], Chun-Yao Niu[1], Chong Li[1], Jun-Hyung Cho[1,3]* and Yu Jia[1]*

Abstract

We present first-principles density-functional calculations for the structural, electronic, and magnetic properties of substitutional 3*d* transition metal (TM) impurities in two-dimensional black and blue phosphorenes. We find that the magnetic properties of such substitutional impurities can be understood in terms of a simple model based on the Hund's rule. The TM-doped black phosphorenes with Ti, V, Cr, Mn, Fe, and Ni impurities show dilute magnetic semiconductor (DMS) properties while those with Sc and Co impurities show nonmagnetic properties. On the other hand, the TM-doped blue phosphorenes with V, Cr, Mn, and Fe impurities show DMS properties, with Ni impurity showing half-metal properties, whereas Sc- and Co-doped systems show nonmagnetic properties. We identify two different regimes depending on the occupation of the hybridized electronic states of TM and phosphorous atoms: (i) bonding states are completely empty or filled for Sc- and Co-doped black and blue phosphorenes, leading to nonmagnetic; (ii) non-bonding *d* states are partially occupied for Ti-, V-, Cr-, Mn-, Fe- and Ni-doped black and blue phosphorenes, giving rise to large and localized spin moments. These results provide a new route for the potential applications of dilute magnetic semiconductor and half-metal in spintronic devices by employing black and blue phosphorenes.

PACS numbers: 73.22.-f, 75.50.Pp, 75.75.+a

Keywords: Dilute magnetic semiconductor, Half-metal, Transition metal doping, Phosphorene

Background

Two-dimensional (2D) materials, graphene and silicene, are currently the subject of intense theoretical and experimental research especially for their novel electronic device applications [1, 2]. Graphene and silicene have demonstrated many exquisite phenomena originating from the characteristic conical dispersion and chiral behavior of their valence and conduction bands around the Fermi level [3, 4]. Generally speaking, the nanostructures of graphene and silicene such as nanoribbons, nanotubes,

and their interconnections have opened new routes for experimental and theoretical studies in the field of nano-electronics [5]. Very recently, black phosphorene, a single layer of black phosphorus (BP), was successfully fabricated through exfoliation from the bulk black phosphorus [6] and therefore becomes, besides graphene and silicene, another stable elemental 2D material. The black phosphorene presents some advantages superior to other previously studied 2D semiconductors because of its intriguing electronic properties, thereby drawing enormous interest from the society of materials science [7–13]. Recently, Li et al. [14] reported that black phosphorene could be applied to the channel of the field-effect transistor (FET) device that has a high carrier mobility of $\sim 10^3 \mathrm{cm}^2/\mathrm{V} \cdot \mathrm{s}$ and an on/off ratio of $\sim 10^4$ at room temperature. As the allotrope of black phosphorene, blue phosphorene has the

*Correspondence: chojh@hanyang.ac.kr; jiayu@zzu.edu.cn
[1]International Laboratory for Quantum Functional Materials of Henan and School of Physics and Engineering, Zhengzhou University, Zhengzhou 450001, China
[3]Department of Physics and Research Institute for Natural Sciences, Hanyang University, 17 Haengdang-Dong, Seongdong-Ku, Seoul 133-791, Korea
Full list of author information is available at the end of the article

Springer

Yu *et al. Nanoscale Research Letters* (2016) 11:77

Page 2 of 9

same stability as black phosphorene at room temperature, and its band gap is larger than black phosphorene [15]. These good electronic properties of black and blue phosphorene nanosheets can be useful for the development of future nanoelectronic devices, spintronics, and related applications [16–23].

For the design of practical electronic devices, defects and impurities have been employed to tune the electrical, optical, and other properties. Over the last decades, the resulting dilute magnetic semiconductors (DMS) and half-metals have achieved important developments both in fundamental aspects and prospective technological applications [24, 25]. Indeed, it was possible to understand the underlying mechanisms of interaction between dilute magnetic impurities allowing ferromagnetic semiconductors at room temperature. For prospective applications, the integration between 2D semiconductors and magnetic data storage enables the development of two-dimensional spintronic devices such as spin valve, spin-based transistors, non-volatile magnetoresistive memories, and even magnetically enhanced optoelectronics devices.

Meanwhile, in spite of the success of 2D materials such as graphene, silicene, transition metal dichalcogenides (TMDCs) [26], and black phosphorene [17, 27, 28], there has been rare study on the dilute magnetic characters of doped 2D black phosphorene except the work of Hashmi et al. [29] and Sui et al. [30], while half-metal properties in doped blue phosphorene have remained unexplored so far. From a technical point of view, 2D semiconductors have other superior factors that can be exploited in magnetic or spintronic devices. First, the carrier concentration can be externally controlled by voltage gating. Secondly, there is room to improve the control of the impurity concentration, for example, by employing adatoms as impurities with concentrations above the solubility limit. In practice, studies of magnetic semiconductor nanostructures with lower dimensionalities, including semiconductor nanocrystals and nanowires doped with transition metals (TM), demonstrated that the confinement effect and the improved control of magnetic dopants can be used to increase the Curie temperature [31].

In this work, we focus on substitutional $3d$ TM impurities (from Sc to Ni) in black and blue phosphorenes to investigate their dilute magnetic characters and half-metal properties. Using first-principles density functional theory (DFT) calculations, we study the structural, electronic, and magnetic properties of substitutional $3d$ TM impurities in black and blue phosphorenes. One of our key results is that the electronic and magnetic properties of these substitutional impurities can be understood by a simple model based on the hybridization between the TM d orbitals and the defect (i.e., phosphorous vacancy) levels. This model together with the calculated band structure provides an explanation for the non-trivial behaviors

of the binding energy and the spin moments for all the systems considered. Concisely, we distinguish two different regimes that depend on the electron filling of TM-phosphorous hybridized levels: (i) completely unoccupied (occupied) bonding states for Sc (Co) lead to nonmagnetic and (ii) partially occupied non-bonding d shell for Ti, V, Cr, Mn, Fe, and Ni give rise to large and localized spin moments.

This paper is organized as follows. After a brief description of the computational details, we present the geometry structures, binding energies, and magnetic properties of all the substitutional TM impurities studied. We also present the general ideas behind our model of the metal-phosphorus hybridization in the considered systems. Then, the electronic structure of the unreconstructed C_{2h}^3 phosphorus vacancy in pristine phosphorene, along with the electronic structures of the different groups of impurities, are presented. Finally, we give a summary with some general conclusions.

Methods

The present DFT calculations were performed using the Vienna Ab initio Simulation Package (VASP) code with a plane-wave basis set [32]. Projector augmented wave (PAW) potentials [33] were used to describe the core electrons, and the generalized gradient approximation (GGA) of Perdew, Burke, and Ernzernhof (PBE) [34] was adopted for exchange-correlation energy. To examine the reliability of the PBE method on the magnetic properties of the black and blue phosphorenes containing $3d$ TM impurity atoms, we also considered the effect of the on-site Coulomb interaction U on the magnetic property within the PBE + U method. The values of U are 4.0, 5.5, 3.3, 3.5, 4.3, 3.3, and 6.5 eV for Sc-, Ti-, V-, Cr-, Mn-, Fe-, Co-, and Ni-doped systems, respectively. The kinetic energy cutoff of the plane-wave basis set used was 500 eV, and for the structural optimization, convergence of Hellmann-Feynman residual forces less than 0.01 eV/Å per atom was achieved. Because the convergence with respect to the number of k-points was especially critical to obtain accurate results for the spin moment in the systems studied, we used an adequate number of k-points for all the different supercell sizes, equivalent to $9 \times 9 \times 1$ Monkhorst-Pack [35] sampling. The Fermi level was smeared by the Gaussian method with a width of 0.05 eV. Most of our results were obtained using $2 \times 2/4 \times 4$ crystallographic symmetrical supercells of black and blue phosphorenes, with a doping concentration of 3.13 %, as shown in Fig. 1a, b. We also checked the results by performing calculations using larger supercells up to $4 \times 4/6 \times 6$ [concentration of 1.56(1.39) %] for several elements. In order to avoid spurious interactions between periodic images of the defective phosphorene layer, a vacuum spacing perpendicular to the plane was employed to be larger than ∼15 Å.

Yu *et al. Nanoscale Research Letters* (2016) 11:77

Page 3 of 9
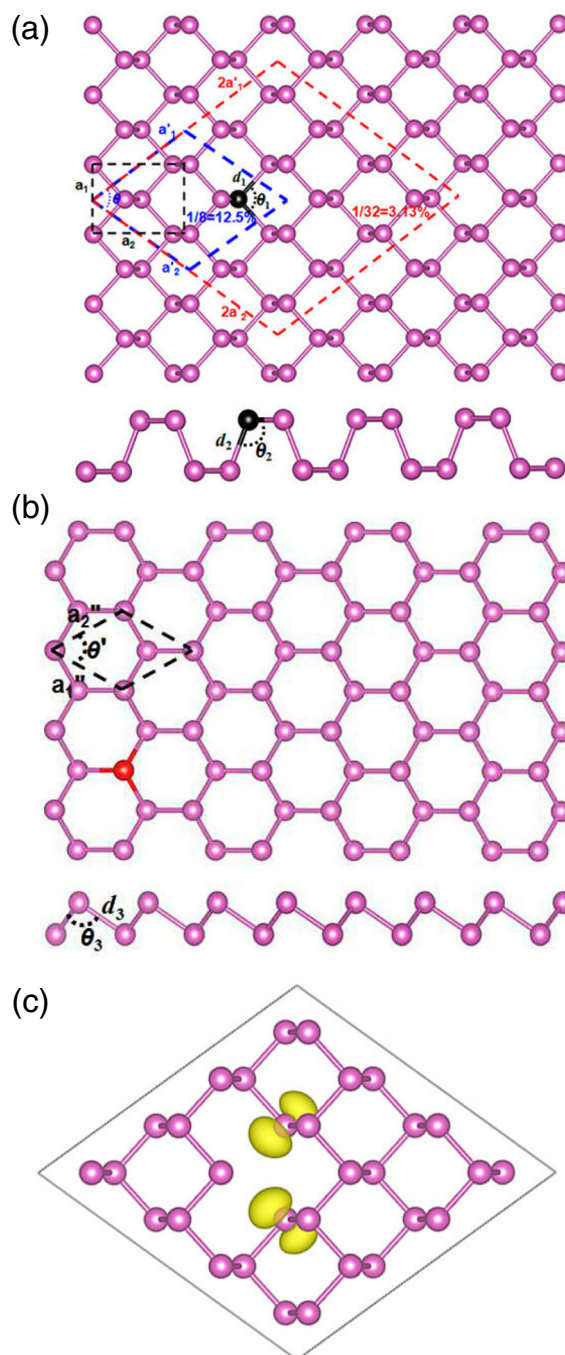
Fig. 1 a Top and side views of a diamond-like 2 × 2 supercell of black phosphorene used in the present calculations. **b** Top and side views of blue phosphorene. **c** Spin density of black phosphorene containing a vacancy with an isosurface of 0.25 e/Å³

Results and Discussion

Geometrical Parameters and Binding Energies

The typical structure of the systems studied in this paper is presented in Fig. 1. Figure 1a shows the diamond-like 2 × 2 supercell structure of monolayer black phosphorene, with a doping concentration of 3.13 %. In view of symmetry and doping isotropy, the diamond-shape unit cell was employed instead of the rectangle unit cell. As shown in Fig. 1a, the optimized lattice constants are $a_1 = 3.310$ Å, $a_2 = 4.589$ Å, and $a'_1 = a'_2 = \left(a_1^2 + a_2^2\right)^{1/2} = 5.658$ Å, and the angle between the basis vectors a'_1 and a'_2 is 71.89°. These values are consistent with experiment and other theoretical calculations [36]. Figure 1b displays the optimized structure of the blue phosphorene with lattice constants

Yu *et al. Nanoscale Research Letters* (2016) 11:77

Page 4 of 9

$a_1'' = a_2'' = 3.330$ Å, and their angle $\theta' = 60°$, which are in good agreement with previous DFT calculations [15].

We begin to study pure black and blue phosphorenes with a monovacancy. Because the blue phosphorene with monovacancy has no magnetism, we only plot the spin charge density of the black phosphorene with monovacancy in Fig. 1c. Figure 1c shows the spin density of black phosphorene with a monovacancy. Similar to the carbon atoms around the vacancy in graphene, the phosphorus atoms around the vacancy in phosphorene undergo a Jahn-Teller distortion, and two of the phosphorus atoms close to the vacancy site move towards each other to form a P-P distance of 1.832 Å, which is 0.408 Å smaller than that of the intrinsic phosphorene. The ground state of the system has a magnetic moment of 1.00 μB/unit cell, most of which is concentrated at the two P atoms with the unsaturated bonds, as seen in Fig. 1c.

The structural parameters and energetic properties of the substitutional TMs in black and blue phosphorenes are shown in Fig. 2. For TM-doped black phosphorene, the bond angles θ_1 and θ_2 monotonically increase from Sc to Ni (see Fig. 2b). Meanwhile, the bond lengths d_1 and d_2 decrease for Sc-, Ti-, and V-doped systems and increase for Cr-doped system, decrease again for Mn-, Fe-, and Co-doped systems, and then increase for Ni-doped system (see Fig. 2a). These behaviors of the bond lengths and bond angles reflect the size of the TM atoms. As for TM-doped blue phosphorene, the bond length d_3 decreases

from Sc to Mn and then increases from Mn to Ni (see Fig. 2d), while the band angle θ_3 shows an oscillating behavior (see Fig. 2e).

Figure 2c shows the calculated binding energies (E_b) of the TM-doped black phosphorenes, where E_b is defined as $-(E_{total}-E_{phosphorene}-E_{atom})$. Here, E_{total} is the energy of the whole configuration, $E_{phosphorene}$ is the energy of the phosphorene with a vacancy, and E_{atom} represents the energy of an isolated dopant atom. We find a continuous increase of the binding energy from Sc to Cr, and then decrease from Mn to Ni, and the binding energies for the considered TMs are in the range of 0.375–5.466 eV. Interestingly, Cr-doped system has the maximum binding energy. This peculiar behavior is related with the interplay between the energy down-shift and the compression of the 3d shell of the TM as the atomic number increases. Although this explanation will be more clear when the metal-phosphorus hybridization levels are discussed below, we note that the behavior of the binding energies of the substitutional 3d TM arises from two competing effects:

(i) From Sc to Cr, the decrease of d_1 and d_2 reflects an increase in the bonding strength between the TM and phosphorous atoms

(ii) From Mn to Ni, as the 3d shell is occupied, its hybridization with the phosphorous vacancy states is weakened to decrease the binding energy
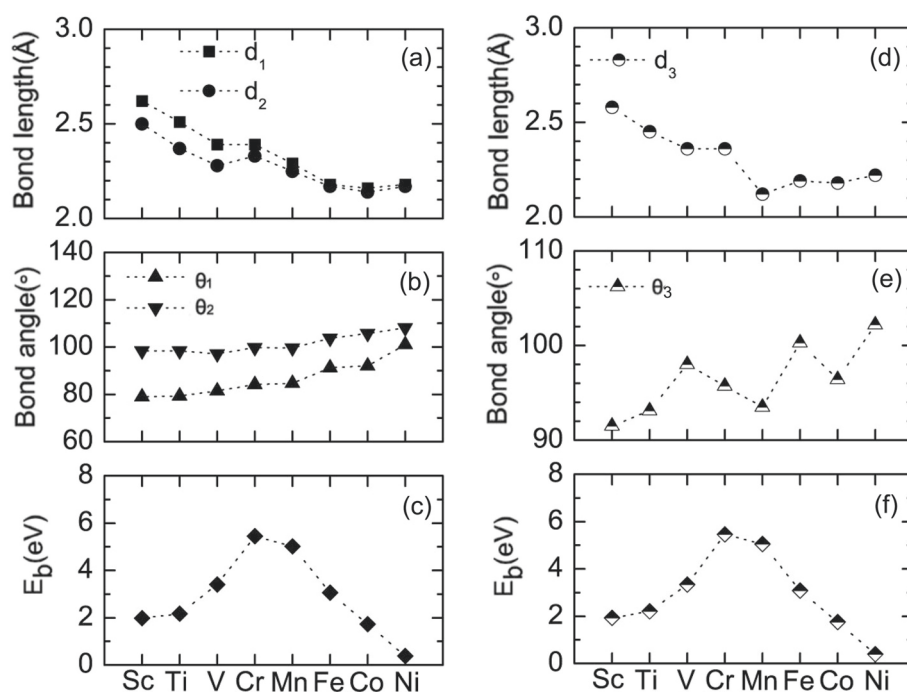
Fig. 2 a, **b** Structural parameters and **c** binding energies of the substitutional TM-doped black phosphorenes. The corresponding ones of the substitutional TM-doped blue phosphorenes are given in **d**, **e**, and **f**

Yu *et al. Nanoscale Research Letters* (2016) 11:77

Page 5 of 9

It is noticeable that this trend of the energetics for the TM-doped black phosphorenes is very similar to that for the TM-doped blue phosphorenes (see Fig. 2f).

Spin Moments

The spin moments of substitutional TMs in black and blue phosphorenes are displayed in Fig. 3a, together with those of the isolated TM atoms. We find that the spin moments of the isolated TM atoms are 1, 3, 5, 6, 5, 4, 3, and 2 μB from Sc to Ni, respectively. On the other hand, the TM-substituted black phosphorenes have the zero magnetic moment for Sc and Co, but 1, 2, 3, 2, 1, and 1 μB for Ti, V, Cr, Mn, Fe, and Ni, respectively, which are the same as the corresponding cases in blue phosphorene. For both of the TM-substituted black and blue phosphorenes, we analyze the charge transfer using Bader charge (see Table 1). We find that for both cases, the TM atoms lose electron charges while the nearest phosphorous atoms gain electron charges. It is notable that the magnitudes of gained and lost charges decrease as the atomic number increases.
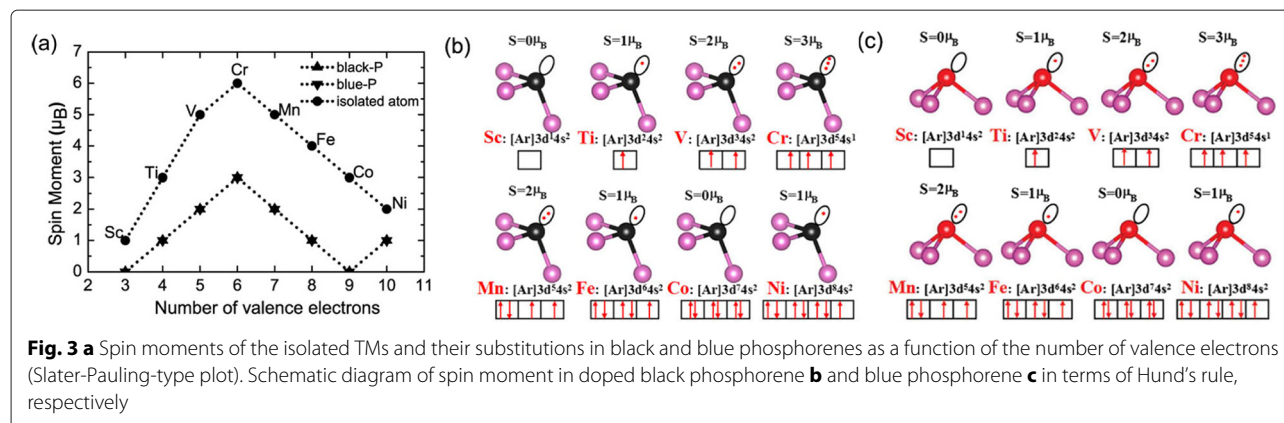
Interestingly, as shown in Fig. 3a, the total spin moments have the integer values of 0, 1, 2, 3, 2, 1, 0, and 1 μB for Sc-, Ti-, V-, Cr-, Mn-, Fe-, Co-, and Ni-doped black and blue phosphorenes, respectively. According to a first-principles study of substitutional TM impurities in graphene, the spin moments are calculated to be 0, 0, 1, 2, 3, 2, 1, and 1 μB for Sc-, Ti-, V-, Cr-, Mn-, Fe-, Co-, and Ni-doped graphene systems, respectively. These values are well compared with 0, 1, 2, 3, 2, 1, 0, and 1 μB for Sc-, Ti-, V-, Cr-, Mn-, Fe-, Co-, and Ni-doped black and blue phosphorenes, respectively. It is interesting to note that the spin moment of each TM impurity (except Sc and Ni) in graphene is smaller by 1 μB compared to the corresponding one in black and blue phosphorenes. This may be attributed to the different bonding natures of graphene and phosphorene: i.e., sp^2 bonding in graphene and sp^3 bonding in phosphorene. Since one valence electron of TM impurities in graphene participates in π bonding with neighboring C atoms, the spin moment is likely to

decrease by 1 μB. To understand this deeply, we draw the schematic diagram of spin moment according to Hund's rule in Fig. 3b. We here note that the valence electron configurations of Sc, Ti, V, Cr, Mn, Fe, Co, and Ni are $3d^14s^2$, $3d^24s^2$, $3d^34s^2$, $3d^54s^1$, $3d^54s^2$, $3d^64s^2$, $3d^74s^2$, $3d^84s^2$, respectively. Briefly, we can distinguish the several regimes depending on the filling of electronic levels:

(i) Sc-doped black phosphorene have the empty Sc-phosphorous bonding levels, leading to a zero spin moment.
(ii) Co-doped black phosphorene have fully occupied Co-phosphorous bonding levels, leading to a zero spin moment.
(iii) Ti-, V-, and Cr-doped black phosphorene have partially occupied TM-phosphorous bonding levels with the spin moments of 1.00, 2.00, and 3.00 μB, respectively.
(iv) Mn-, Fe-, and Ni-doped black phosphorene have partially occupied non-bonding 3d levels with the spin moments of 2.00, 1.00, and 1.00 μB.

It is notable that the spin moments of TM-doped blue phosphorene (see Fig. 3c) are the same as those of black phosphorene because the energy states of s and d in the outermost orbital of TM atoms and phosphorus atom are very close to each other.

To explore the underlying mechanism of the magnetic moments in TM-doped black and blue phosphorenes, the Mulliken population analysis was performed to list the results in Table 2. We find that the spin moments of the TM impurities (S_M) have a dominant contribution for the nearest phosphorus neighbors (S_{P1} and S_{P2}). The calculated spin moments of TM impurities for Ti, V, Cr, Mn, Fe, and Ni in doped black phosphorene are $S_M = 0.986, 1.977, 3.082, 2.207, 1.097,$ and 0.953 μB, respectively, close to the above-discussed Hund's analysis. Similarly, the spin moments of TM impurities for Ti, V, Cr, Mn, Fe and Ni in doped blue phosphorenes

Fig. 3 a Spin moments of the isolated TMs and their substitutions in black and blue phosphorenes as a function of the number of valence electrons (Slater-Pauling-type plot). Schematic diagram of spin moment in doped black phosphorene **b** and blue phosphorene **c** in terms of Hund's rule, respectively

Yu *et al. Nanoscale Research Letters* (2016) 11:77

Page 6 of 9

Table 1 Electronic charges of each atomic species in the TM-doped black and blue phosphorenes, obtained using Bader charge analysis. The positive (negative) sign represents the gained (lost) electrons

	Atoms	Sc	Ti	V	Cr	Mn	Fe	Co	Ni
Black-P	TM	−1.54	−1.23	−0.97	−0.87	−0.61	−0.37	−0.19	−0.16
	Nearest-P	+0.97	+0.78	+0.59	+0.59	+0.33	+0.12	+0.09	+0.07
Blue-P	TM	−1.55	−1.27	−1.05	−0.88	−0.57	−0.40	−0.21	−0.20
	Nearest-P	+0.98	+0.79	+0.63	+0.60	+0.31	+0.13	+0.10	+0.09

are $S_M = 0.992, 2.032, 3.147, 1.954, 1.247$ and, 0.967 μB, respectively.

Analysis of the Electronic Structures

Before the analysis of the electronic structures of TM-doped black and blue phosphorene, we first examine the electronic structure of a single phosphorous vacancy in black phosphorene. As substitutional impurities in black phosphorene, most of the TM atoms studied here exhibit a symmetrical configuration of C_{2h}^3 [37]. For this reason, it is particularly instructive to analyze their electronic structures with the hybridization between the atomic levels of the TM atoms and those associated with a relaxed C_{2h}^3 symmetrical phosphorus vacancy. As shown in Fig. 4, the C_{2h}^3 vacancy shows a considerable spin polarization of 1.00 μB, indicating a dilute magnetic property.

To further shed light on the underlying mechanism of magnetic properties in the TM-doped black and blue phosphorene structures, we plot the spin-polarized band structures of TM-doped black and blue phosphorenes in Fig. 5a, b, respectively. Interestingly, the majority and minority spin bands for Ti-, V-, Cr-, Mn-, Fe-, and Ni-doped black phosphorene show semiconducting characters (see Fig. 5a), indicating dilute magnetic properties. On the other hand, Sc- and Co-doped black phosphorene exhibit zero spin moment, whereas Ti- and Ni-doped blue phosphorene show half-metal characters (see Fig. 5b). Note that V-, Cr-, Mn-, and Fe-doped blue phosphorenes exhibit dilute semiconducting characters, while Sc- and Co-doped blue phosphorenes have zero spin moment.

Generally, substitutional TM impurities in black and blue phosphorenes exhibit very similar behaviors in their energetic and magnetic properties. This result indicates that the structural differences of black- and blue-phosphorene lattices are insensitive to determine the energetic and magnetic properties of TM-doped black and blue phosphorenes, as shown in Figs. 2, 3, and 5.

It is interesting to examine the effect of the on-site Coulomb interaction U on the magnetic properties of the

Table 2 Spin moments in the TM impurity (S_M) and the nearest phosphorus neighbors (S_{P1} and S_{P2}) for different substitutional TMs in black and blue phosphorenes

	Doped-atom	S_M (μB)	S_{P1} (μB)	S_{P2} (μB)	S_{tot} (μB)	E_g (eV)
Black-P	Sc				0.00	0.97 (1.36)
	Ti	0.986	−0.014	−0.017	1.00	0.36 (0.90)
	V	1.977	−0.001	−0.002	2.00	0.07 (0.09)
	Cr	3.082	−0.076	−0.085	3.00	0.72 (0.93)
	Mn	2.207	−0.053	−0.060	2.00	0.39 (0.82)
	Fe	1.097	−0.036	−0.019	1.00	0.27 (0.90)
	Co				0.00	0.61 (1.08)
	Ni	0.953	0.064	−0.007	1.00	0.09 (0.46)
Blue-P	Sc				0.00	1.35 (1.59)
	Ti	0.992	−0.020	−0.020	1.00	0 (0.73)
	V	2.032	−0.055	−0.055	2.00	0.15 (0.47)
	Cr	3.147	−0.083	−0.083	3.00	0.91 (1.63)
	Mn	1.954	−0.032	−0.020	2.00	0.12 (0.73)
	Fe	1.247	−0.044	−0.044	1.00	0.35 (0.91)
	Co				0.00	0.69 (1.12)
	Ni	0.967	0.039	0.039	1.00	0 (0)

S_{tot} is the total spin moment of the doped black and blue phosphorenes. The band gaps (E_g) of TM-doped black (blue) phosphorenes are also given. The values in parentheses are the PBE + U band gaps
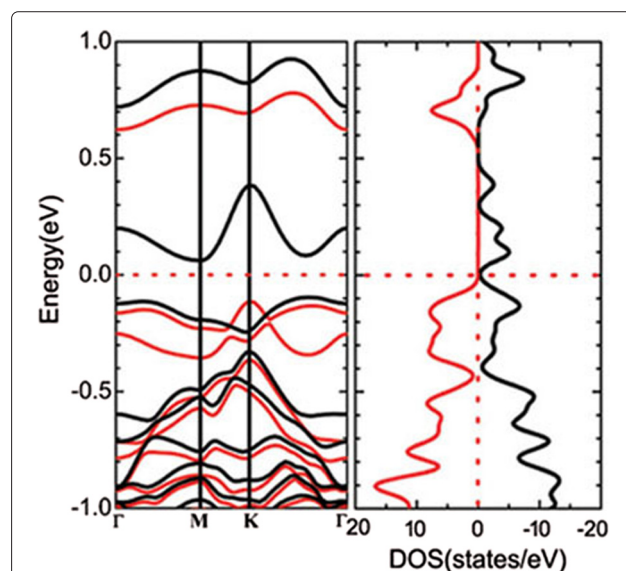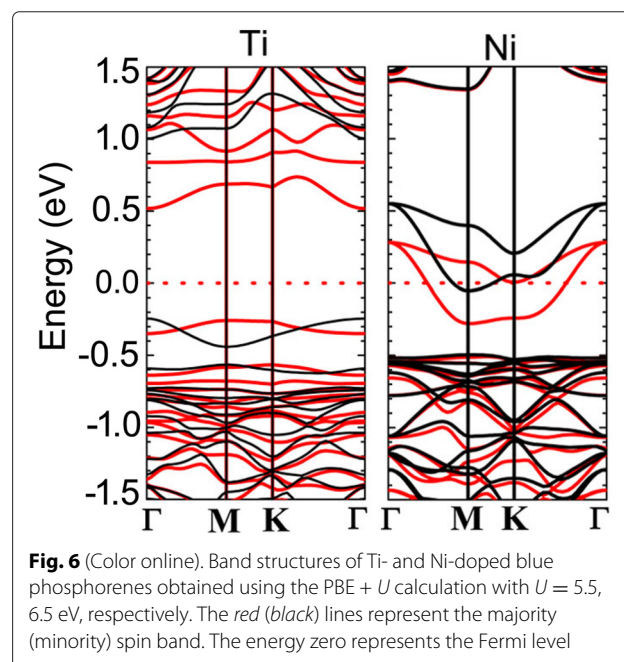

Fig. 4 (Color online). Band structure and density of states of the undoped defective black phosphorene. The *red* lines represent majority spin band, while the *black* lines represent minority spin band. The energy zero represents the Fermi level

Yu *et al. Nanoscale Research Letters* (2016) 11:77

Page 7 of 9

Fig. 5 (Color online). Band structures of Sc-, Ti-, V-, Cr-, Mn-, Fe-, Co- and Ni-doped *black* (**a**) and *blue* (**b**) phosphorenes, respectively. The *red* (*black*) lines represent the majority (minority) spin band. The energy zero represents the Fermi level
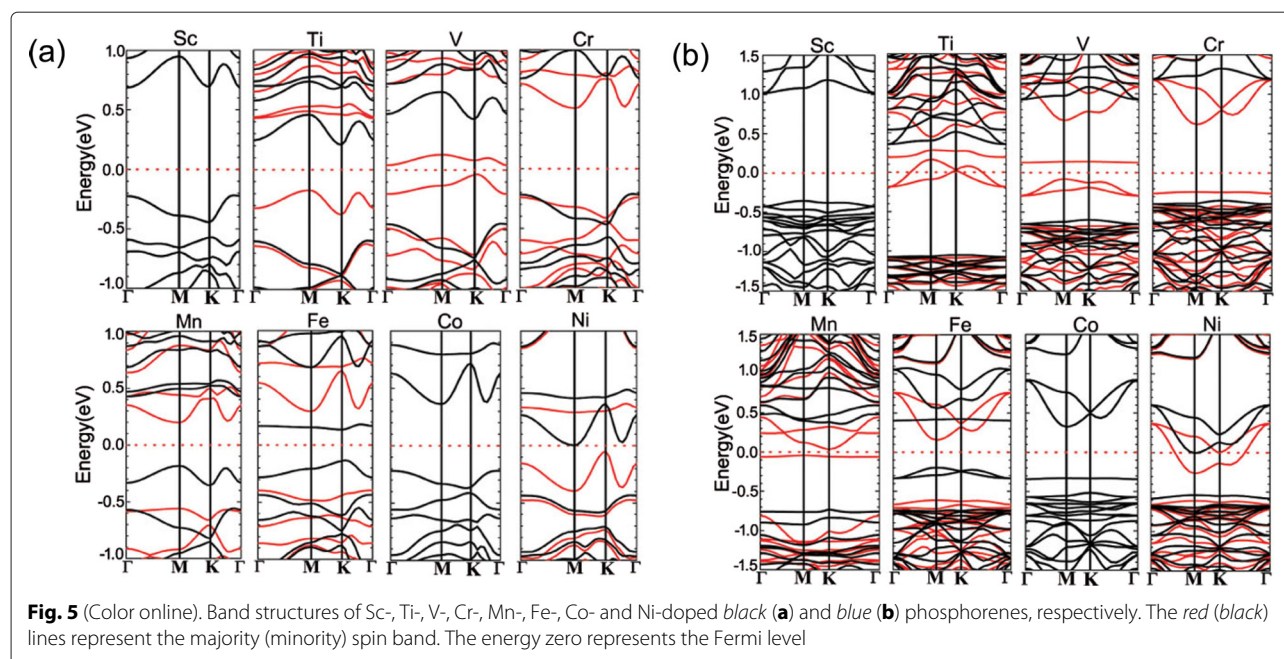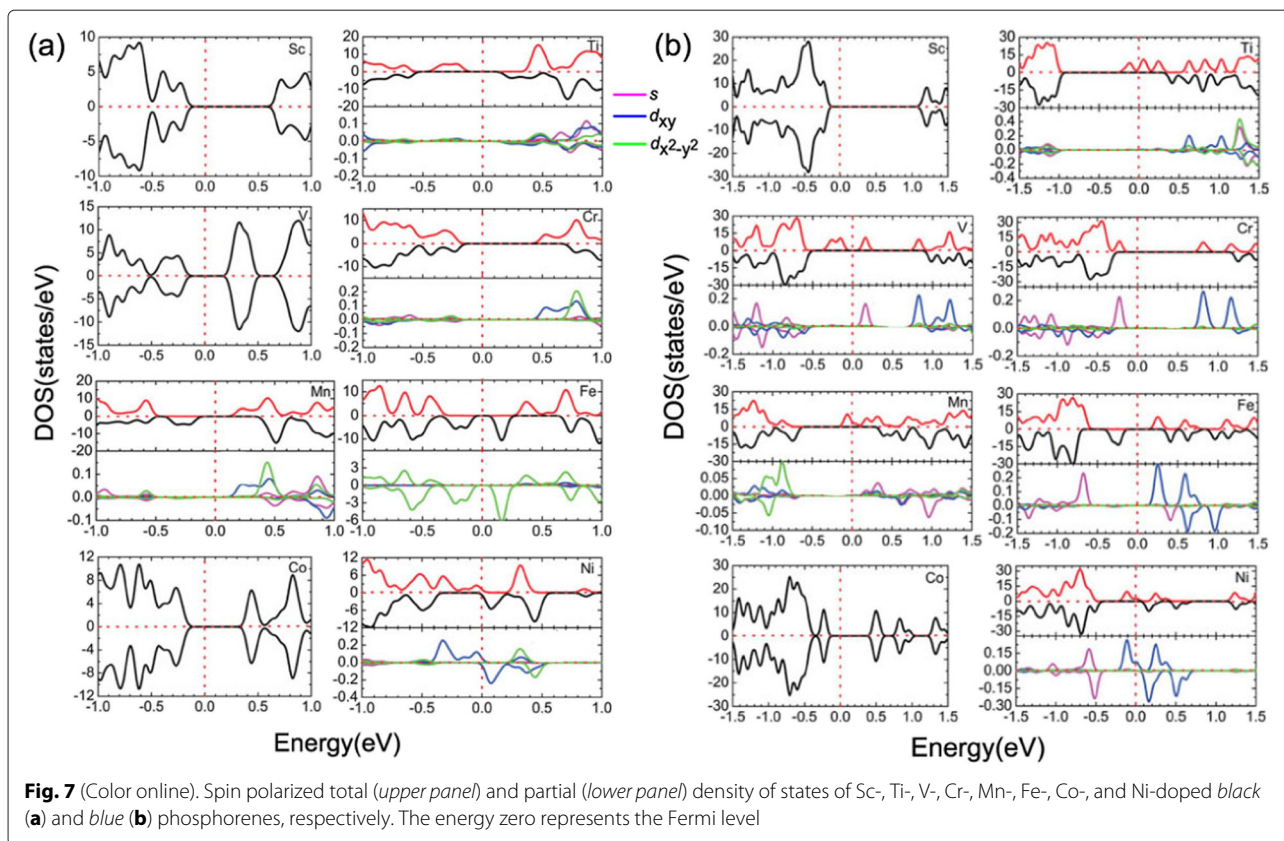
substitutional $3d$ TM impurities in black and blue phosphorenes. We perform the PBE + U calculations for all the considered systems, where the values of U = 4.0, 5.5, 3.3, 3.5, 3.5, 4.3, 3.3, and 6.5 eV are chosen for Sc-, Ti-, V-, Cr-, Mn-, Fe-, Co-, and Ni-doped systems, respectively [38–40]. The calculated PBE + U band gaps (Eg) of Sc-, Ti-, V-, Cr-, Mn-, Fe-, Co-, and Ni-doped black and blue phosphorenes are listed in Table 2. We find that Eg of the magnetic semiconductor obtained using PBE + U increases by ∼30 % compared to the PBE results. However, it is noticeable that the spin moment does not change depending on the PBE and PBE + U methods. Interestingly, we find that the PBE + U band structure of Ti-doped blue phosphorene shows a magnetic semiconductor property with a gap opening (see Fig. 6), different from the half-metallic character predicted by PBE. This indicates that U in Ti-doped blue phosphorene splits the narrow half-filled bands crossing the Fermi level into lower and upper Hubbard bands. On the other hand, the half-metallic character of Ni-doped blue phosphorene predicted by PBE is preserved in the PBE + U band structure (see Fig. 6), because the bands crossing the Fermi level have relatively larger band widths compared to those in Ti-doped blue phosphorene (see Fig. 5b).

A general picture of the dilute magnetic and half-metal features of the TM-doped black and blue phosphorenes can be seen from the analysis of the spin-polarized total and partial DOS, as shown in Fig. 7. As for Sc- and Co-doped black phosphorenes, the total DOS of the majority and minority states are completely compensated with each other, yielding zero spin moment (see Fig. 7a). It is found that for Ti-, V-, Cr-, Mn-, Fe- and Ni-doped

black phosphorenes, the total DOS of the majority and minority states are not compensated below E_F and show a gap opening, indicating dilute magnetic semiconducting properties. We note that the DOS of Sc- and Co-doped blue phosphorene show nonmagnetic properties; those of Ti- and Ni-doped blue phosphorene show half-metal properties; V-, Cr-, Mn-, and Fe-doped blue phosphorenes show dilute magnetic semiconductor characters (see Fig. 7b). From the analysis of the spin-polarized total and

Fig. 6 (Color online). Band structures of Ti- and Ni-doped blue phosphorenes obtained using the PBE + U calculation with U = 5.5, 6.5 eV, respectively. The *red* (*black*) lines represent the majority (minority) spin band. The energy zero represents the Fermi level

Yu *et al. Nanoscale Research Letters* (2016) 11:77

Page 8 of 9

Fig. 7 (Color online). Spin polarized total (*upper panel*) and partial (*lower panel*) density of states of Sc-, Ti-, V-, Cr-, Mn-, Fe-, Co-, and Ni-doped *black* (**a**) and *blue* (**b**) phosphorenes, respectively. The energy zero represents the Fermi level

partial DOS, it is seen that the magnetic moments are well localized at the TM atom site, and the d_{xy} and $d_{x^2-y^2}$ orbitals are dominant for the contribution to the partial DOS.

Conclusions

We have performed a first-principles DFT calculation for the structural, energetic, and magnetic properties of a series of substitutional $3d$ TM impurities in black and blue phosphorenes. We provided a simple model based on Hund's rule for understanding the calculated electronic and magnetic properties of the considered systems, where the dilute-semiconducting and half-metal features, spin moment, and binding energy are varied depending on the atomic number of the TM atoms. The spin-polarized band structures and DOS calculations show that for black phosphorene, the Ti-, V-, Cr-, Mn-, Fe-, and Ni-doped systems have dilute magnetic semiconductor properties, while Sc- and Co-doped systems have no magnetism. For blue phosphorene, the Ni-doped system shows half-metal properties, while V-, Cr-, Mn-, and Fe-doped systems show dilute magnetic semiconductor characters, Sc- and Co-doped systems show non-magnetism.

Since substitutional impurities of $3d$ TM atoms in black and blue phosphorenes exhibit some intriguing electronic and magnetic properties, such doped systems can provide

an interesting route to tune various functions for spin electronic devices based on black and blue phosphorenes. This functional ability together with the high stability of substitutional impurities can open a route to fabricate ordered arrays of these impurities at predefined locations, which would allow the experimental tests of the theoretical predictions of unusual magnetic interactions mediated by black and blue phosphorenes.

Authors' contributions
YJ and J-HC conceived the idea. WY performed the calculations, analyzed the data, and wrote the manuscript. ZZ, C-YN and CL also participated in the discussions of the calculated results. All the authors have read and approved the final manuscript.

Author details
[1] International Laboratory for Quantum Functional Materials of Henan and School of Physics and Engineering, Zhengzhou University, Zhengzhou 450001, China. [2] School of Physics and Chemistry, Henan Polytechnic University, Jiaozuo 454000, China. [3] Department of Physics and Research Institute for Natural Sciences, Hanyang University, 17 Haengdang-Dong, Seongdong-Ku, Seoul 133-791, Korea.

Yu *et al. Nanoscale Research Letters* (2016) 11:77

Page 9 of 9

References

1. Geim AK, Grigorieva IV (2013) Van der Waals heterostructures. Nature 499:419
2. Vogt P, Padova PD, Quaresima C, Avila J, Frantzeskakis E, Asensio MC, Resta A, Ealet B, Lay GL (2012) Silicene: compelling experimental evidence for graphenelike two-dimensional silicon. Phy Rev Lett 108:155501
3. Bianco E, Butler S, Jiang S, Restrepo OD, Windl W, Goldberger E (2013) Stability and exfoliation of germanane: a germanium graphane analogue. ACS Nano 7:4414
4. Butler SZ, Hollen SM, Cao L, Cui Y, Gupta JA, et al (2013) Progress, challenges, and opportunities in two-dimensional materials beyond graphene. ACS Nano 7:2898
5. Zhang S, Li C, Li SF, Sun Q, Guo ZX, Jia Y (2014) Intrinsic spin dependent and ferromagnetic stability on edge saturated zigzag graphene-like carbon-nitride nanoribbons. Appl Phys Lett 104:172111
6. Reich ES (2014) Phosphorene excites materials scientists. Nature 506:19
7. Zhu ZL, Li C, Yu WY, Chang DH, Sun Q, Jia Y (2014) Magnetism of zigzag edge phosphorene nanoribbons. Appl Phys Lett 105:113105
8. Tran V, Soklaski R, Liang YF, Yang L (2014) Layercontrolled band gap and anisotropic excitons in few-layer black phosphorus. Phys Rev B Phys 89:235319
9. Fei RX, Yang L (2014) Strain-engineering the anisotropic electrical conductance of few-layer black phosphorus. Nano Lett 14:2884
10. Fei RX, Yang L (2014) Lattice vibrational modes and Raman scattering spectra of strained phosphorene. Appl Phys Lett 105:083120
11. Tranm V, Yang L (2014) Unusual scaling laws of the band gap and optical absorption of phosphorene nanoribbons. Phys Rev B 89:245407
12. Zhu ZL, Yu WY, Ren XY, Sun Q, Jia Y (2015) Grain boundary in phosphorene and its unique roles on C and O doping. Europ Lett 109:47003
13. Yu WY, Zhu ZL, Niu CY, Li C, Cho JH, Jia Y (2015) Anomalous doping effect in black phosphorene using first-principles calculations. Phys Chem Chem Phys 17:16351
14. Li L, Yu Y, Ye GJ, Ge Q, Ou X, Wu H, Feng D, Chen XH, Zhang YB (2014) Black phosphorus fieled-effect transistors. Nat Nanotech 9:372
15. Zhu Z, Tomanek D (2014) Semiconducting layered blue phosphorus: a computational study. Phys Rev Lett 112:176802
16. Buscema M, Groenendijk DJ, Blanter SI, Steele GA, Van der Zant HSJ, Gomez AC (2014) Fast and broadband photoresponse of few-layer black phosphorus field-effect transistors. Nano Lett 14:3347
17. Cai YQ, Ke QQ, Zhang G, Zhang YW (2015) Energetics, charge transfer, and magnetism of small molecules physisorbed on phosphorene. J Phys Chem C 119:3102
18. Kulish VV, Malyi OI, Perssonc C, Wu P (2015) Adsorption of metal adatoms on single-layer phosphorene. Phys Chem Chem Phys 17:992
19. Kulish VV, Malyi OI, Persson C, Wu P (2015) Phosphorene as an anode material for Na-ion batteries: a first-principles study. Phys Chem Chem Phys 17:13921
20. Boukhvalov DW, Rudenko AN, Prishchenko DA, Mazurenko VG, Katsnelson MI (2015) Chemical modifications and stability of phosphorene with impurities: a first principles study. Phys Chem Chem Phys 17:15209
21. Qin GZ, Yan QB, Qin ZZ, Yue SY, Hu M, Su G (2015) Anisotropic intrinsic lattice thermal conductivity of phosphorene from first principles. Phys Chem Chem Phys 17:4854
22. Liu X, Wen YW, Chen ZZ, Shan B, Chen R (2015) A first-principles study of sodium adsorption and diffusion on phosphorene. Phys Chem Chem Phys 17:16398
23. Zheng HL, Zhang JM, Yang BS, Du XB, Yan Y (2015) A first-principles study on the magnetic properties of nonmetal atom doped phosphorene monolayers. Phys Chem Chem Phys 17:16341
24. Zhu ZL, Chen WG, Sun Q, Jia Y (2014) Half-metal behaviour mediated by self-doping of topological line defect combining with adsorption of 3*d* transition-metal atomic chains in graphene. J Phys D 47:055303
25. Feng Y, Ji WX, Huang BJ, Chen XL, Li F, Li P, Zhang CW, Wang PJ (2015) The magnetic and optical properties of 3*d* transition metal doped SnO_2 nanosheets. RSC Adv 5:24306
26. Wang QH, Kalantar-Zadeh K, Kis A, Coleman JN, Strano MS (2012) Low frequency electronic Noise in single-layer MoS_2 transistors. Nat Nanotechnol 7:699
27. Hu T, Hong JS (2015) First-principles ptudy of metal adatom adsorption on black phosphorene. J Phys Chem C 119:8199
28. Khan I, Hong JS (2015) Manipulation of magnetic state in phosphorene layer by non-magnetic impurity doping. New J Phys 17:023056
29. Hashmi A, Hong J (2015) Transition metal doped phosphorene: first-principles study. J Phys Chem C 119:9198
30. Sui XL, Si C, Shao B, Zou XL, Wu J, Gu BL, Duan WH (2015) Tunable magnetism in transition-metal-decorated phosphorene. J Phys Chem C 119:10059
31. Seixas L, Carvalho A, Castro Neto AH (2015) Atomically thin dilute magnetism in Co-doped phosphorene. Phys Rev B 91:155138
32. Kresse G, Furthmller J (1996) Efficiency of ab-initio total energy calculations for metals and semiconductors using a plane-wave basis set. Comput Mater Sci 6:15
33. Blochl PE (1994) Projector augmented-wave method. Phys Rev B 50:17953
34. Perdew JP, Burke K, Ernzerhof M (1996) Generalized gradient approximation made simple. Phys Rev Lett 77:3865
35. Monkhosrt HJ, Pack JD (1976) Special points for Brillouin-zone integrations. Phys Rev B 13:5188
36. Qiao JS, Kong XH, Hu ZX, Yang F, Ji W (2014) High-mobility transport anisotropy and linear dichroism in few-layer black phosphorus. Nat Comm 5:4475
37. Ribeiro SJ, Almeida RM, Cancado LG, Dresselhaus MS, Jorio A (2015) Group theory for structural analysis and lattice vibrations in phosphorene systems. Phys Rev B 91:205421
38. Rai DP, Thapa RK (2013) An ab initio study of the half metallic properties of Co_2TGe (T = Sc, Ti, V, Cr, Mn, Fe): LSDA + U method. J Korean Phys Soc 62:1652
39. Huang WL, Zhu Q, Ge W, Li H (2011) Oxygen-vacancy formation in $LaMO_3$ (M = Ti, V, Cr, Mn, Fe, Co, Ni) calculated at both GGA and GGA + U levels. Comput Mater Sci 50:1088
40. Pari G, Mathi Jaya S, Subramoniam G, Asokamani R (1995) Density-functional descriytion of the electronic structure of $LaMO_3$ (M = Sc, Ti, V, Cr, Mn, Fe, Co, Ni). Phys Rev B 51:16575